Catalysis Science & Technology

ROYAL SOCIETY OF CHEMISTRY

PAPER

View Article Online
View Journal | View Issue

Cite this: *Catal. Sci. Technol.*, 2024, **14**, 1216

The formation, reactivity and transformation pathways of formaldehyde in the methanol-to-hydrocarbon conversion†

Vladimir Paunović, *[a] Xiangkun Wu,[b] Luca Maggiulli,[ab] Davide Ferri,[b] Patrick Hemberger,[b] Andras Bodi[b] and Jeroen A. van Bokhoven *[ab]

Received 27th December 2023,
Accepted 17th January 2024

DOI: 10.1039/d3cy01786a

rsc.li/catalysis

Coke-induced catalyst deactivation is one of the major challenges in commercial methanol-to-hydrocarbon (MTH) conversion processes. It is suspected to be critically dependent on formaldehyde-mediated reactions. Using photoelectron photoion coincidence and *operando* diffuse reflectance UV-vis spectroscopy techniques, we reveal details of formaldehyde formation and reactivity over industrially relevant ZSM-5 catalysts, and its role in the coke formation. We show that in the early stage of the MTH reaction, formaldehyde is mainly obtained *via* methanol disproportionation, with a moderate apparent activation energy of 70 kJ mol^{-1}. In the fully developed reaction phase, it readily converts alkenes into dienes and aliphatic polyenes, which are then promptly converted to methylbenzenes, naphthalenes, and polycyclic arenes that compose coke. We evidence increased reactivity of formaldehyde and dienes over catalysts exhibiting higher productivity of arenes and high propensity to coking. The results suggest that the consumption of this intermediate is not only dependent on the concentration of Brønsted acid sites, but also on their nature, the presence of Lewis acid sites, and framework defects. A high reactivity of cyclopentadienes towards formaldehyde and detection of fulvenes indicate their involvement as key intermediates in the transformation of alkenes to akylbenzenes. The identification of styrene and indene derivatives suggests a pathway to polycyclic arenes by condensation of formaldehyde with aliphatic substituents on arene rings, followed by cyclization. The results demonstrate the pivotal role of formaldehyde in the MTH reaction.

Introduction

Methanol-to-hydrocarbon (MTH) conversion over molecular sieve catalysts is an important technology for the production of light alkenes, aromatics, and fuels from a range of fossil and renewable alternatives to petroleum.[1–3] After fast methanol–dimethyl ether (DME) equilibration and evolution of the first C_{2+} species, C–C bonds are assembled *via* methylation and cracking reactions of the alkene- and arene-based chain carriers, which can be interconverted *via* hydrogen transfer (HT) and cyclization reactions.[1–5] This unique array of reactions is referred to as the dual-cycle hydrocarbon pool (DCHP) mechanism. It proceeds *via* carbenium ion intermediates formed by the interaction of hydrocarbon chain carriers with Brønsted acid sites (BAS) in the confined micropore space.[1,3–5] The cracking of alkene chain carriers results in the formation of propene and higher alkenes, whereas arene-mediated reactions produce ethene, propene, and mono- and bicyclic methylated aromatics. However, MTH reaction sequences also yield higher molecular weight by-products, predominantly alkylated polycyclic aromatic hydrocarbons (PAHs).[1,6–12] The impaired diffusion and strong adsorption of PAHs on BAS lead to their accumulation in the form of internal (micropore) and external coke deposits, causing MTH catalyst deactivation.[7–9,11,12] Catalyst coking is the central challenge in the MTH conversion, because coke limits the catalyst turnover capacity, dissipates a substantial part of up to 8% of the methanol feed, and introduces the need for high-temperature catalyst regeneration that causes permanent structural degradation of the catalysts.[6,11,12]

The formation of coke species is primarily associated with HT reactions, which convert alkenes into conjugated aliphatics, *i.e.*, dienes and polyenes, arenes, and finally PAHs, in order of increasing thermodynamic stability.[12,13] Methanol and DME, *i.e.*, surface methoxy-groups, are highly potent hydrogen donors in addition to unsaturated

[a] *Institute for Chemical and Bioengineering, ETH Zurich, Vladimir-Prelog-Weg 1, 8093 Zurich, Switzerland. E-mail: vladimir.paunovic@chem.ethz.ch, jeroen.vanbokhoven@chem.ethz.ch*
[b] *Paul Scherrer Institute, Forschungsstrasse 111, 5232 Villigen, Switzerland*
† Electronic supplementary information (ESI) available. See DOI: https://doi.org/10.1039/d3cy01786a

hydrocarbons, such as alkenes. In methanol-induced HT (MIHT), hydride is abstracted by another methoxy or carbenium ion, which is thus converted into methane or C_{2+} alkanes, respectively.[14–20] An important outcome of MIHT is the dehydrogenation of methanol to formaldehyde. Previous reports showed that the yield of formaldehyde decreases with the progress of the MTH reaction over a ZSM-5 catalyst, almost vanishing at high conversions.[17] Moreover, a prominent increase in arene formation and catalyst coking propensity was reported in the presence of a formaldehyde co-feed.[13,21] The alkene cycle and catalyst stability are enhanced under the conditions that either minimize MIHT,[13,21] promote the decomposition of formaldehyde,[22] or reduce its reactivity.[23,24] It has been proposed that formaldehyde promotes the formation of dienes, polyenes, and aromatics *via* Prins condensation and/or hydroacylation reaction with alkenes,[13,17,21] as well as diphenylmethane formation *via* condensation with arene chain carriers.[25] All these steps are catalyzed by BAS.[18] These findings imply that the product distribution and the coking propensity of the MTH catalysts critically depend on their activity for formaldehyde formation and subsequently, formaldehyde-mediated reactions (FMRs). In particular, zeolites exhibiting high acid site density are expected to be more reactive in formaldehyde formation and FMRs than their low-acidity counterparts,[13,17] which may explain the higher arene selectivity and decreased stability of the former compared to the latter.[26–28] However, the relationships between formaldehyde formation and reactivity, product distribution, and catalyst stability have not been systematically explored so far, and the FMR reaction intermediates remain elusive.

In this study, formaldehyde evolution and reactivity were assessed over several ZSM-5 catalysts with varying acidity and MTH catalytic performance by photoelectron photoion coincidence (PEPICO) spectroscopy, which enables fragmentation-free and isotope- and isomer-specific detection of molecules at high sampling frequency.[20,29–34] Formaldehyde co-feeding and isotope labeling PEPICO spectroscopy experiments were complemented with *operando* diffuse reflectance UV-vis (DRUV-vis) spectroscopic analysis of the zeolite-confined intermediates, and by the assessment of deactivating potential of different species *via* co-feeding experiments. Thus, we gained a thorough picture of formaldehyde formation and FMRs by identifying the reactive intermediates and uncovering the relationships between the formaldehyde reactivity and catalytic performance. The results verify the prominent role of formaldehyde in the evolution of aromatics and coke-forming reactions.

Results and discussion

Kinetics of formaldehyde formation in the MTH conversion

The kinetics of formaldehyde formation in the MTH process was investigated over Z_{40} and CaZ_{40} zeolites by using a PEPICO spectroscopy set-up (Fig. S1†). Z_{40} is a prototypical MTH catalyst, which is composed of *ca.* 0.4–1 μm particles and exhibits moderate acidity (Fig. S2, S3 and Table S1†). The incorporation of alkaline-earth counterions such as calcium enables the concentration and strength of BAS to be substantially reduced (Fig. S3, Table S1†), without modifying the particle size and significantly altering the distribution of defects in the material.[28,34] In addition, CaZ_{40} serves as a pertinent model material for analyzing the potential influence of extra-framework calcium cations on the formaldehyde formation in the MTH reaction. This is particularly noteworthy because the incorporation of calcium significantly diminishes the production of arenes,[28,34] which may arise from reduced generation of this intermediate compound. Owing to their medium and low BAS densities, respectively, these Z_{40} and CaZ_{40} catalysts display reduced methanol conversion activities (Fig. 1a and S4†). This, along with their operation at increased WHSV, permits the study of the MTH reaction in the low conversion regime that limits the consumption of formaldehyde in subsequent reactions with hydrocarbons.[17,19] The evolution of formaldehyde and other species in the reactor outlet stream was assessed by PEPICO spectroscopy (Fig. S1†). The formaldehyde ion (m/z 30) was detected at a photon energy of $h\nu$ = 10.9 eV, slightly above its ionization potential (IP = 10.88 eV, Fig. 1a and S1†).[20,35] Its identity was unequivocally confirmed by recording photoionization (PI) and photoion mass-selected threshold photoelectron (ms-TPE) spectra (Fig. S1†). The onset of formaldehyde formation over the Z_{40} and CaZ_{40} catalysts was observed at *ca.* 625 K (Fig. 1a and b). This was paralleled by the appearance of methane (m/z 16, $h\nu$ = 13.6 eV), which was the only observable hydrocarbon at low temperatures (Fig. 1a). With increasing temperature, the production of formaldehyde and methane increased, and signals associated with ethene (m/z 28), propene (m/z 42), and butene (m/z 56) started to evolve, implying the formation of the HP (Fig. 1a and c). Nonetheless, the carbon-based yields of detected light alkenes (*ca.* 0.8% in total) were lower than those of methane and formaldehyde (*ca.* 2.2%, Fig. 1c), indicating that MIHT still prevailed over the reactions of the hydrocarbon pool. Notably, alkanes, such as propane (m/z 44) and butane (m/z 58), methylated benzenes (MBs), such as methylbenzene (1 MB, m/z 92) and dimethylbenzene (2 MB, m/z 106), and dienes, such as butadiene (m/z 54), were not detected under these reaction conditions (Fig. 1a). The lack of alkanes in the outlet reactor feed indicates the absence of MIHT to alkenes and points that methanol disproportionation being the main pathway of the formaldehyde formation.[17] This is further corroborated by the equivalent yields of formaldehyde and methane, which is in good agreement with the reaction stoichiometry (Fig. 1c). The absence of dienes and arenes, which are the expected products of the formaldehyde-mediated reaction sequences such as Prins condensation,

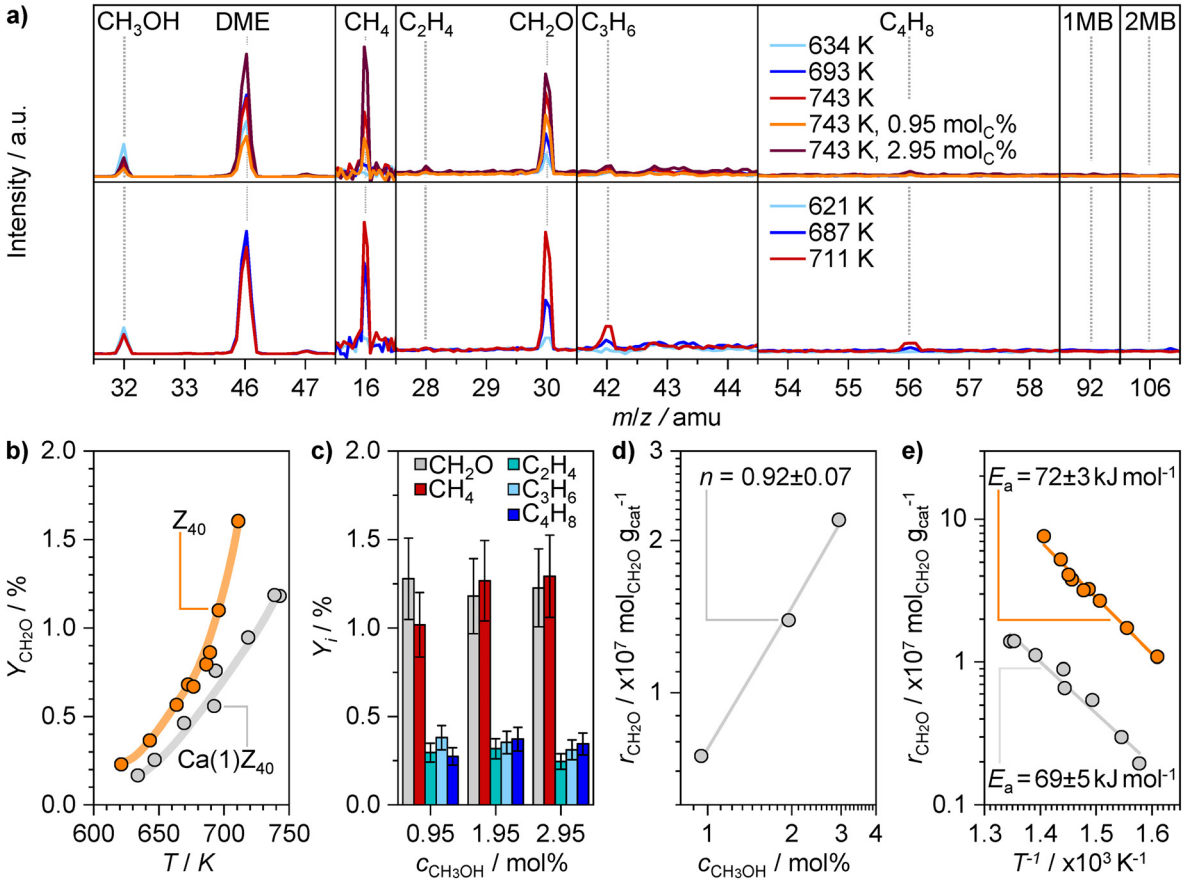

Fig. 1 (a) Mass spectra of reactive species detected in the MTH reaction over CaZ_{40} (top) and Z_{40} (bottom) catalysts at various temperatures and methanol concentrations. The spectra were recorded at $h\nu$ = 10.9 eV, except for that of methane, which was recorded at $h\nu$ = 13.6 eV. (b) Formaldehyde yield *vs.* temperature over CaZ_{40} and Z_{40}. (c) Formaldehyde yield and hydrocarbon products over CaZ_{40} at different inlet methanol concentrations. Apparent rates of formaldehyde formation *vs.* (d) methanol concentration over CaZ_{40} and (e) temperature over CaZ_{40} and Z_{40}. Methanol variation experiments were performed at 743 K. The estimated apparent reaction order and activation energies are indicated in the plots. All products were detected and quantified by PEPICO spectroscopy. Reaction conditions: CH_3OH : Xe : Ar = 1.95(0.95 or 2.95) : 0.15 : 97.9(98.9 or 96.9) mol%, WHSV = 1.4 (CaZ_{40}) or 5.4 (Z_{40}) g_{CH_3OH} g_{cat}^{-1} h^{-1}, T = 621–743 K, and P = 0.4 bar.

suggests that subsequent formaldehyde conversion is greatly suppressed (Fig. 1c).[15,17] Formaldehyde may be also consumed through the reactions leading to the formation of HP intermediates, which are expected to propagate the formation of the C_{2+} hydrocarbons. However, the measurement of the catalytic performance of the CaZ_{40} catalyst showed that its activity and product distribution remained unaltered over longer reaction time, which indicates that the concentration of HP species does not change significantly (Fig. S5†). In addition, as shown in the example of the CaZ_{40} catalyst, the yields of detectable products are invariant to the inlet methanol concentration, indicating that the formation of formaldehyde and methane, as well as the synthesis of light alkenes, exhibits a first-order dependence with respect to this reactant (Fig. 1c and d). The apparent order of formaldehyde formation of *ca.* 1 is in agreement with the mechanism in which the hydride transfer occurs between the surface-bound methyl species and weakly bound methanol molecule (please see ESI† Discussion S2.1).[18] The methanol-to-DME ratio at different inlet methanol concentrations remained constant and was close to the equilibrium ratio (*ca.* 0.5). These conditions allow us to determine the apparent activation energy of formaldehyde evolution to be *ca.* 70 kJ mol^{-1} over both the Z_{40} and CaZ_{40} catalysts (Fig. 1e). This value is significantly lower than the value estimated by theoretical calculations (*ca.* 130–220 kJ mol^{-1})[18,19] and is comparable to the typical activation barriers for the alkylation of alkene and arene chain carriers (40–80 kJ mol^{-1}).[36–39] Therefore, the kinetics of formaldehyde formation is competitive with that of alkene evolution in the low conversion regime. It is interesting to note that the apparent rates of formaldehyde evolution over the Z_{40} catalyst are *ca.* 7.2× higher than those over the CaZ_{40} catalyst. This activity difference is significantly higher than the ratio of the total BAS, 4.6, in these two catalysts and is comparable to the ratio of their strong BAS concentrations, 8.3 (Table S1†). This suggests that strong BAS are primarily responsible for methanol disproportionation, and that extra-framework calcium ions do not affect this reaction.

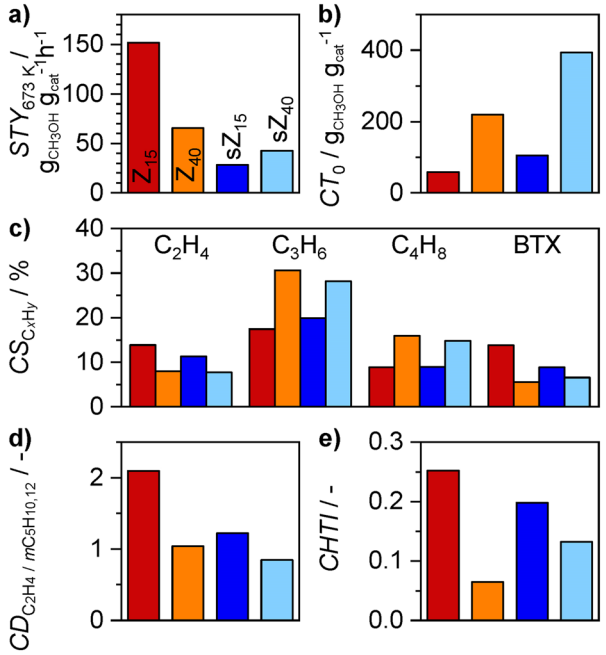

Fig. 2 (a) Space–time yields and (b) cumulative turnover capacities, (c) cumulative selectivities to selected hydrocarbon products, (d) cumulative ethene : (2-methylbutane + 2-methylbutene) ratios and (e) cumulative hydrogen transfer indices of the Z_{15} and Z_{40}, and steamed sZ_{15}, and sZ_{40} catalysts in the MTH reaction. The space–time yield was assessed at 673 K, and other parameters were determined at 773 K. The cumulative product distribution parameters were calculated in the 20–95% conversion range. The complete selectivity–conversion profiles of the catalysts are presented in Fig. S6.† All reactants and products were detected and quantified by the GC-FID method. The color code in (a) applies to all plots. Other conditions: CH_3OH : Ar = 19 : 81 mol%, WHSV = 76 or 253 (Z_{15} at 673 K) $g_{CH_3OH}\ g_{cat}^{-1}\ h^{-1}$, and P = 1.6 bar.

Relationship between the MTH performance and formaldehyde reactivity

After analyzing the formaldehyde evolution in the initial stages of the MTH reaction, its yield and the relationship with the MTH catalytic performance were investigated in a broader range of conversions. Commercial Z_{15} and Z_{40} zeolites were selected as representative model catalysts because of their distinct MTH performance (Fig. 2, S4 and S6†). Scanning electron microscopy (SEM) shows that both Z_{15} and Z_{40} catalysts contain particles of similar size (0.4–1 μm, Fig. S1 and S2†). Besides, they also exhibit very similar textural properties (Table S1†). The most prominent difference between the Z_{15} and Z_{40} samples is in their acid properties, wherein the former sample contains much higher concentration of BAS and LAS. The highly acidic Z_{15} zeolite displays higher MTH activity (STY, Fig. 2a), lower cumulative turnover capacity (CT_0, Fig. 2b), and higher propensity to form ethene and aromatics with respect to C_{3+} alkenes than its less acidic Z_{40} counterpart (Fig. 2c, S3 and S4†). Such a performance profile implies that the arene chain carriers are more abundant over Z_{15} than over Z_{40}, which is reflected by the higher ethene : (2-methylbutane + 2-methylbutene) ratio ($D_{C_2H_4/mC_5H_{10,12}}$, Fig. 2d).[40] Consistently, Z_{15} displayed a higher propensity for catalyzing HT reactions than Z_{40}, inferred from the higher selectivities to methane and the higher fraction of C_{2-4} alkanes relative to the total amount of C_{2-4} hydrocarbon products and as expressed by the hydrogen transfer index (HTI, Fig. 2e).[41]

In view of previous findings indicating that MIHT is the prevailing HT mechanism at sub-complete conversion and suggesting that formaldehyde strongly affects the MTH reaction mechanism,[12,15,17,20,22] it is relevant to compare the formaldehyde concentration profiles over these two materials as a function of methanol conversion, which was adjusted by gradually increasing the reactor temperature. Although PEPICO catalytic experiments were performed at lower pressures than laboratory tests because of the high sensitivity and arrangement of the detection system, all the catalysts were active in a characteristic temperature window of the MTH reaction of *ca.* 580–730 K, wherein their light-off curves follow the order of activities assessed in a conventional lab-based fixed-bed reactor (Fig. S4†). The performance of Z_{15} and Z_{40} was compared at a constant contact time per total BAS (τ_{BAS}) concentration and at a constant WHSV. In line with the established catalytic role of BAS in MTH conversion, the Z_{15} and Z_{40} catalysts displayed almost identical sigmoidal light-off profiles at a constant τ_{BAS} in the *operando* PEPICO experiment (Fig. 3a). Consistent with the fixed-bed catalytic tests (Fig. 2 and S6†), the Z_{40} catalyst displayed a higher selectivity to C_{3+} alkenes (Fig. 3d–f) and a lower selectivity to ethene (Fig. 3c), alkanes (Fig. 3k), and MBs (Fig. 3m–o), demonstrating that the product distribution trends are preserved in the PEPICO experiments.

PEPICO spectroscopy enables quantitative monitoring of the changes in the yield of formaldehyde along with other characteristic MTH products (Fig. 3b–o) and analysis of the relationships in their evolution. Herein, different structural isomers of C_{4+} products could be identified based on PI and photoion ms-TPE spectra (Fig. S7†). In agreement with the observation that formaldehyde is the primary reaction intermediate that readily reacts with different MTH species, the yield of formaldehyde increases in the lower and decreases in the higher conversion range, attaining an almost zero value at near complete conversion levels (Fig. 3b). After a similar increase up to conversion levels of *ca.* 6%, the formaldehyde yield over the Z_{15}, τ_{BAS} catalyst is *ca.*1.5× higher than the one over Z_{40} in the conversion range up to *ca.* 40%. This is accompanied by the higher yield of C_4 and C_5 alkanes over Z_{15}, τ_{BAS} with respect to the Z_{40} catalyst in this conversion range, suggesting that the higher yield of formaldehyde over the Z_{15}, τ_{BAS} catalyst arises from the more prominent MIHT between methanol and alkenes. In the case of the Z_{40} catalyst, a decrease of the formaldehyde yield is observable at conversion levels exceeding *ca.* 60%. At this turning point, the yields of acyclic dienes display a pronounced upward trend of the change of the yield (C_4H_6, C_5H_8, Fig. 3g and h), while 1MB and 3MB also display only a small positive inflection. C_4 and C_5 alkenes show a downward curve of the change of the yield at conversions

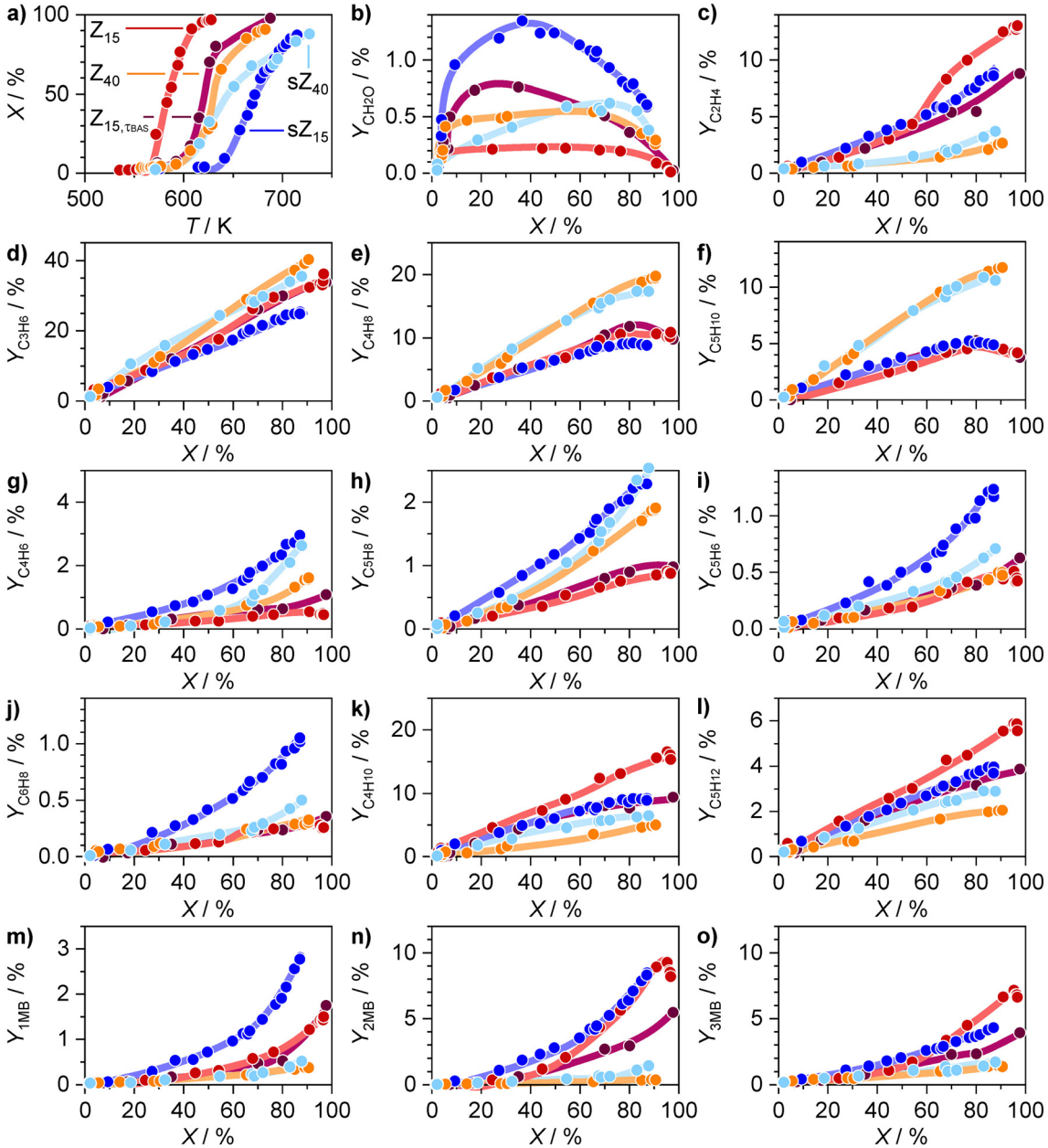

Fig. 3 (a) Conversion *versus* temperature and (b–o) yields of formaldehyde and specific hydrocarbon products *versus* conversion in the MTH reaction over Z_{15} and Z_{40}, and steamed sZ_{15}, and sZ_{40} catalysts as detected by PEPICO spectroscopy. The color code in (a) applies to all plots. Reaction conditions: CH_3OH : Xe : Ar = 1.95 : 0.15 : 97.9 mol%, WHSV = 1.4 or 3.4 (Z_{15}, τ_{BAS}) g_{CH_3OH} g_{cat}^{-1} h^{-1}, T = 537–727 K, and P = 0.4 bar.

above *ca.* 60% (Fig. 3e and f). These trends in changes in the yield indicate that the conversion of formaldehyde over the Z_{40} catalyst is associated with the formation of acyclic dienes, likely *via* the Prins reaction.[17] Consistent with this observation, the Z_{40} catalyst displays *ca.* 2× higher yield of acyclic dienes than Z_{15}, τ_{BAS} (C_4H_6, C_5H_8, Fig. 3g and h). This parallels the *ca.* 2× higher yields of C_{3-5} alkenes over the latter system, which indicates that the higher average concentration of alkenes in the reactor comprising the Z_{40} material favors the reaction of formaldehyde with these products. The yield of formaldehyde over Z_{15}, τ_{BAS} decreases at conversions above *ca.* 40%, displaying a steep decay at conversions above *ca.* 80%. Both inflection points in the formaldehyde yield *versus* conversion curve coincide with the upward changes of the MB yield (Fig. 3m–o). This provides a strong hint that formaldehyde is consumed in the reaction sequences leading to the formation of MBs and/or in reactions with these arenes. Additional insights are obtained from the experiment over the Z_{15} catalyst performed at identical WHSV as the experiment over the Z_{40} material, which corresponds to *ca.* 2.4 higher τ_{BAS}. Because of longer residence time, the light-off curve of the methanol conversion shifted to *ca.* 45 K lower temperature (Z_{15}, Fig. 3a). Notably, the yield of formaldehyde remains

significantly lower than those measured over the same catalyst at higher WHSV (*i.e.*, Z_{15}, τ_{BAS}) and over the Z_{40} catalyst under the same WHSV conditions (Fig. 3b). Since a lower WHSV (*i.e.*, higher τ_{BAS}) favors the production of formaldehyde, as also supported by the higher yields of MIHT products ($C_{4,5}$ alkanes, Fig. 3k and l), the lower integral yield of formaldehyde over Z_{15} with respect to Z_{15}, τ_{BAS} evidences enhanced consumption of this intermediate over the longer catalyst bed. Among the products, 2MB and 3MB display the most pronounced relative gain in yield (Fig. 3n and o), which further supports the hypothesis that the enhanced consumption of formaldehyde is linked with the formation of these arenes and/or reactions with them.

The experiments performed over the Z_{15} and Z_{40} catalysts indicate that the average concentration of formaldehyde across the catalyst bed increases with decreasing τ_{BAS}. In realistic industrial MTH operation, the residence time increases as a result of progressive coke deposition and because of steam-induced hydrolysis of the framework aluminum atoms.[6,26,42] Regarding the latter source of deactivation, we assess the formaldehyde evolution profiles over severely steamed sZ_{15} and sZ_{40} zeolites that can be viewed as aged Z_{15} and Z_{40} catalysts that have been subjected to multiple regeneration cycles. In comparison with their parent materials, both steamed sZ_{15} and sZ_{40} catalysts display lower catalytic activity, higher CT_0 values, and similar selectivity to C_{3-4} alkenes (Fig. 2a–c). While sZ_{40} and Z_{40} catalysts show similar selectivities to ethene and BTX, sZ_{15} exhibits significantly lower selectivity to these products than its parent counterpart. This indicates that the arene cycle is less prevalent in sZ_{15} than in parent Z_{15}, which is also reflected by the lower value of the $CD_{C_2H_4/mC_5H_{10,12}}$ parameter (Fig. 2d). In comparison with Z_{40} and sZ_{40} catalysts, sZ_{15} displays higher selectivities to ethene and BTX and lower selectivities to propene and butene, as well as lower CT_0 values, although its BAS concentration is lower than those measured in the former two zeolites (Table S1†). Since all three catalysts exhibit similar particle-size distribution and porous properties (Fig. S2, Table S1†), this result indicates that the higher formation of HT products such as alkanes and arenes is induced by other factors including the higher concentration of LAS (Table S1†),[15] which can be linked to the higher fraction of extra-framework aluminum species (Fig. S3†). Besides, the FTIR spectra of sZ_{15} indicate a higher relative fraction of internal silanols (Fig. S3†), which are proposed to promote coking.[43]

In view of these structural and performance differences between the steamed and parent zeolites, it was relevant to assess if these variances are also reflected in the formaldehyde reactivity profiles over these catalysts. The PEPICO data show that the formaldehyde yield over sZ_{15} exhibits a prominent maximum at moderate conversions of *ca.* 45%, which is higher than that of the parent Z_{15} material (Fig. 3b). However, at conversions exceeding *ca.* 45%, the formaldehyde yield exhibits a very steep decline, indicating that the reactivity of formaldehyde remains high over the steamed catalyst sample. In contrast, the formaldehyde yield over sZ_{40} increases more steadily and reaches the maximum value at slightly higher conversions than for the parent Z_{40} catalyst (75% *vs.* 65%). Another peculiar feature of steamed zeolites is the higher yield of dienes with respect to their parent counterparts (Fig. 3g–j), indicating that the decrease in BAS concentration impedes the transformations of these conjugated aliphatics. This result, along with the observed longer catalyst lifetime of the steamed samples, is in good agreement with the previous hypothesis that reactions of dienes and formaldehyde have a profound contribution to the formation of heavier aromatics and catalyst coking.[13,21,25]

Impact of formaldehyde on the MTH reactions

The FMRs are additionally evaluated by step-introduction of formaldehyde to the methanol feed ($CH_2O:CH_3OH$ = 0.55 : 1 mol mol^{-1}) over the representative Z_{40} catalyst. This perturbation caused a substantial change in the product distribution (Fig. 4a). In particular, a rapid increase in the formaldehyde peak (*m*/*z* 30) was accompanied by an increase in methanol (*m*/*z* 32) and DME (*m*/*z* 46) signals (Fig. 4b). The total carbon-based conversion of *ca.* 90% was essentially unaltered after the addition of formaldehyde, indicating an approximately first-order reaction response to the added formaldehyde. The reactivity of formaldehyde is additionally studied by introducing ^{12}C formaldehyde ($^{12}CH_2O$) into a ^{13}C methanol ($^{13}CH_3OH$) feed (Fig. 5). The ^{13}C content in formaldehyde, methanol, and DME, as well as in representative hydrocarbon products, such as propene, 2MB, and 3MB, follows a virtually identical trend and eventually reaches a constant value of *ca.* 0.64, which matches that anticipated from the relative ratio between ^{13}C methanol and ^{12}C formaldehyde ($^{12}CH_2O:{}^{13}CH_3OH$ = 0.55 : 1 mol mol^{-1}, eqn (S11) in the ESI†). These results demonstrate prompt interconversion between DME/methanol and formaldehyde, which is faster than the conversion of methanol and formaldehyde to hydrocarbons. DME/methanol–formaldehyde interconversion likely proceeds *via* hydride scrambling between adsorbed methanol and formaldehyde species (eqn (1)).[17]

$$^{12}CH_3OH + {}^{13}CH_2O \rightleftharpoons {}^{12}CH_2O + {}^{13}CH_3OH \quad (1)$$

More insights into the transformation pathways of formaldehyde are obtained by analyzing the changes of the outlet concentrations of the MTH products induced by formaldehyde co-feeding (Fig. 4a). The introduction of formaldehyde induced a decrease of the C_{3+} alkene concentration to between *ca.* 2.3 and 3.3× lower values than those measured prior to formaldehyde addition (Fig. 4b). The concentration drop was more pronounced for longer alkenes (*e.g.*, 2.3× for propene *vs.* 3.3× decrease for hexenes), indicating the higher reactivity of longer alkenes to formaldehyde. Similar to alkenes, the concentrations of

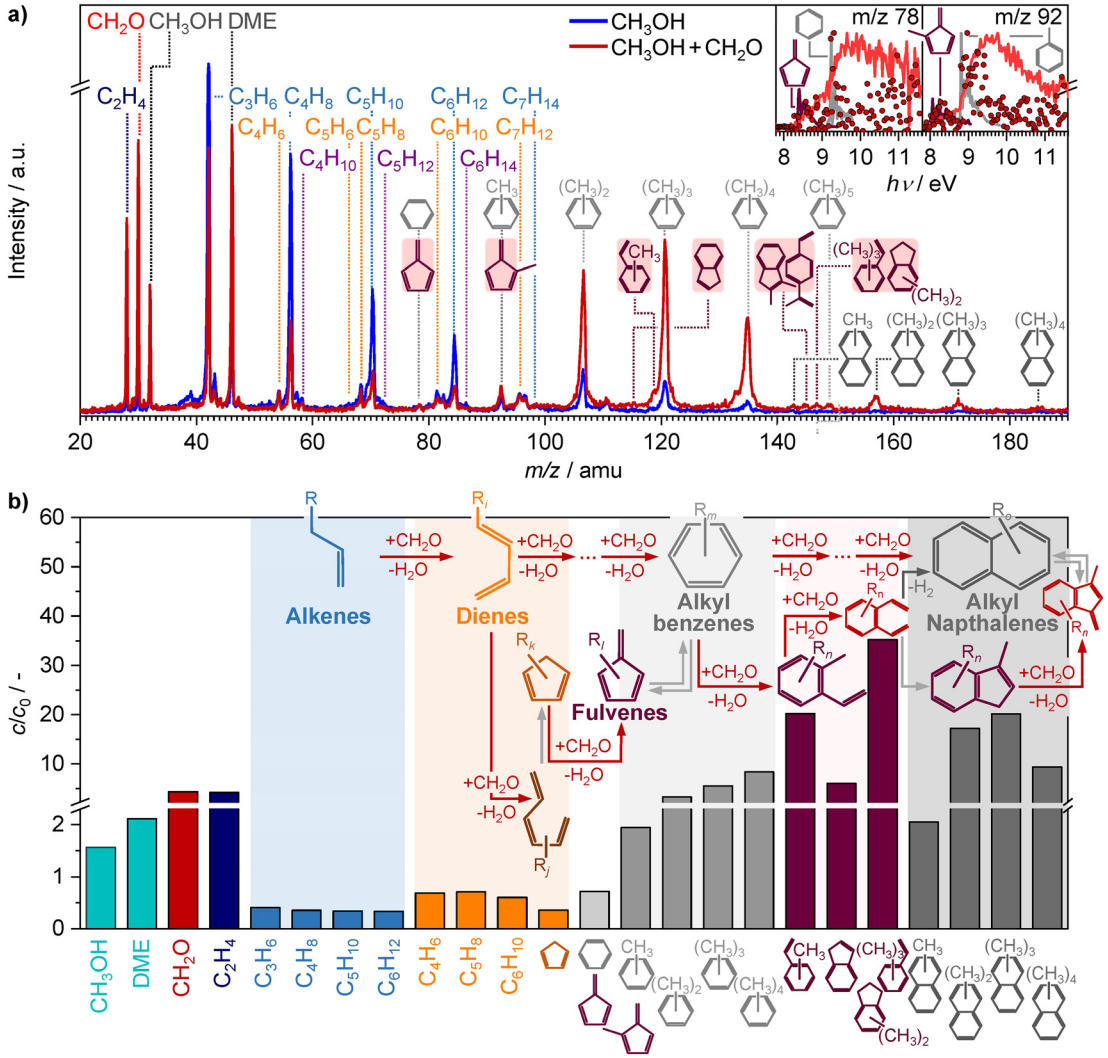

Fig. 4 (a) PEPICO mass spectra of the species detected in the MTH reaction over the Z_{40} catalyst before and 600 s after the addition of the formaldehyde co-feed. The spectra were recorded at $h\nu$ = 10.9 eV. The insets show the photoionization and threshold photoelectron spectra of the *m*/*z* 78 and 92 species along with the reference spectra of (methyl)fulvene and (methyl)benzene. (b) Relative concentration changes of various reaction species induced by introducing the formaldehyde co-feed to the MTH reaction. Formaldehyde-mediated reaction sequences in the conversion of alkenes into arene-based intermediates in the MTH reaction as inferred from the PEPICO and supported by the DRUV-vis results (*vide infra*). Reaction conditions: $CH_3OH : CH_2O : Xe : Ar$ = 1.95 : 0(1.1) : 0.15 : 97.9(96.8) mol%, WHSV = 1.4 g_{CH_3OH} g_{cat}^{-1} h^{-1}, *T* = 678 K, and *P* = 0.4 bar.

acyclic C_{4-8} dienes and cycloalkenes decreased by *ca.* 25–30% (Fig. 4b). The outlet concentration of cyclopentadiene (C_5H_6, *m*/*z* 66) decreased more prominently by *ca.* 60%, which suggests that cyclopentadiene is more reactive towards formaldehyde than its acyclic analogs. In contrast to C_{3+} alkenes and dienes, the addition of formaldehyde strongly enhances the formation of ethene (*ca.* 3.9×), 1 MB/MF (*ca.* 2.1×), 2MB (*ca.* 3.3×), 3MB (*ca.* 5.5×), and 4MB (*ca.* 8.4×, Fig. 4b). A higher relative increase in the rates of 3MB and 4MB evolution with respect to MB implies that FMRs promote the formation of highly methylated arene chain carriers. However, the photoionization and ms-TPE spectra at *m*/*z* 78 and 92 reveal that, in addition to the prevalent benzene (IP = 9.24 eV) and MB (IP = 8.8 eV) species, fulvene (IP = 8.36 eV) and methylfulvene (IP = 8.2 eV) are also present (Fig. 4a, insets and S8†).[30,44] Fulvene derivatives can be produced *via* Prins condensation between (methyl)pentadienes and formaldehyde and can subsequently isomerize into MBs (Fig. 4b, top scheme). The occurrence of this reaction pathway may explain the significantly higher reactivity of cyclopentadiene towards formaldehyde in comparison with its acyclic analogs (Fig. 4b). It is hypothesized that the reactivity of the cyclopentadiene species increases with the extent of the ring alkylation. This may explain the more prominent relative increase of the higher methylated benzene structures in comparison with the small relative change (*ca.* 10%) of the benzene/fulvene (B/F, *m*/*z* = 78) signal upon the addition of formaldehyde (Fig. 4b).

In addition to MBs, the formaldehyde co-feed induced a substantial increase in signals at *m*/*z* 116 (IP = 8.2 eV), 118 (IP = 8.30 eV), 130 (IP = 8.16 eV), 132 (IP = 8.16 eV), and 146 (IP = 7.98 eV, calculated IPs for likely spectral carriers, see

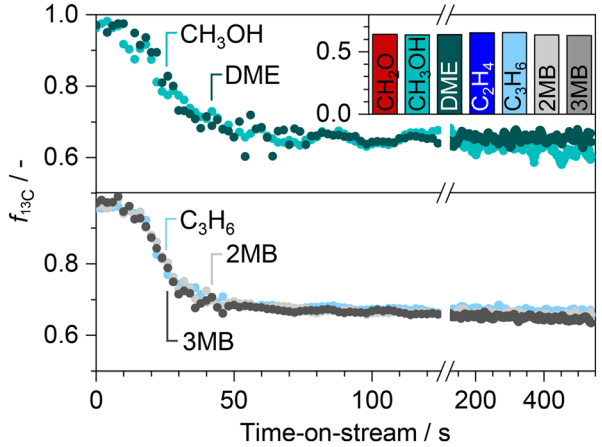

Fig. 5 The fraction of ^{13}C carbon in the representative reaction species after the introduction of formaldehyde to a ^{13}C-labeled methanol feed as detected by PEPICO spectroscopy. The inset shows the ^{13}C fraction after attaining steady state. Reaction conditions are equivalent to those reported in the caption of Fig. 4.

Fig. 4b and S9†). Their ionization profiles indicate that these species likely represent the structural isomers of indene (*m*/*z* 116, 130, 144), indane (*m*/*z* 146), styrene (*m*/*z* 118, 132, 146), and divinylbenzene (*m*/*z* 130), exhibiting different degrees of methylation. Moreover, the species at the high *m*/*z* values of 156, 170, and 184 also increased substantially. Although these species cannot be unequivocally identified, their photoionization onsets (7.8–7.9 eV) and photoionization spectra suggest that they represent alkylated and likely methylated naphthalenes (MNs, Fig. S7†). Notably, the relative increase of the outlet concentrations of styrene (*e.g.*, *m*/*z* 118, *ca.* 6×), indene (*e.g.*, *m*/*z* 116, *ca.* 19×), and indane/styrene (*e.g.*, *m*/*z* 146, *ca.* 34×) species, as well as for MNs (*e.g.*, 3MN *ca.* 20×), is even higher than those observed for most of the MBs (Fig. 4b). This reactivity pattern is consistent with the proposed FMRs in which formaldehyde promotes the transformation of alkenes into MBs, MNs, and PAHs *via* series of sequential steps (Fig. 4b, top scheme). Herein, the alkenes as the starting reactants are expected to display the most prominent decrease, while dienes as the intermediate species that are both formed and consumed are expected to exhibit a lower relative decrease. MBs, indene and styrene species, and MNs, which are positioned in the latter steps of the reaction sequence, are expected to show the most prominent increase in the relative concentration, since their formation is in multiple steps promoted by the addition of the formaldehyde co-feed.

It is further interesting to note that the outlet concentration changes of specific hydrocarbon groups induced by formaldehyde addition follow similar transient profiles (Fig. 6). Herein, the outlet concentrations of alkenes and dienes decrease almost instantaneously with the addition of formaldehyde (phase I, Fig. 6). The onset of MBs and ethene (phase II), indene and styrene species (phase III), and MNs occurs after a certain lag-time (phase IV), which progressively increases with the increases from MBs to MNs.

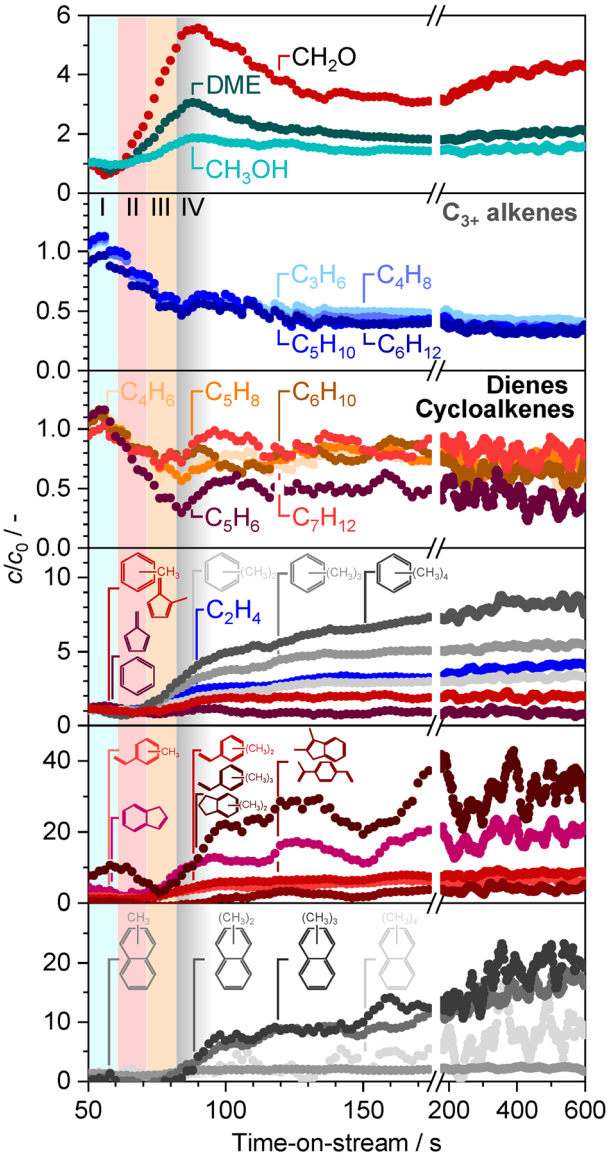

Fig. 6 Temporal evolution of relative concentration changes of various reaction species induced by introducing the formaldehyde co-feed to the MTH reaction as detected by PEPICO spectroscopy. Phases I through IV represent the time periods in which the changes of the outlet concentrations for particular hydrocarbon products commence. Reaction conditions are equivalent to those reported in the caption of Fig. 4.

Considering the integral nature of the MTH reactor under study, the successive onset of various species may also arise from the differences in the micropore diffusivities among various reactants. However, the absence of lag-times among the hydrocarbons of the same group (*e.g.*, between C_3H_6 and C_6H_{12}, 1MB and 4MB) in spite of their different diffusivities (which monotonically increase with molecular weight), and different responses of hydrocarbons displaying comparable diffusivities (*e.g.*, C_2H_6 and C_3H_6, 1MB–3MB and C_{5+} aliphatics) suggest that the transients likely reflect the induction phases of various arene species. Notably, a fast response of alkenes and diene signals and the sequential

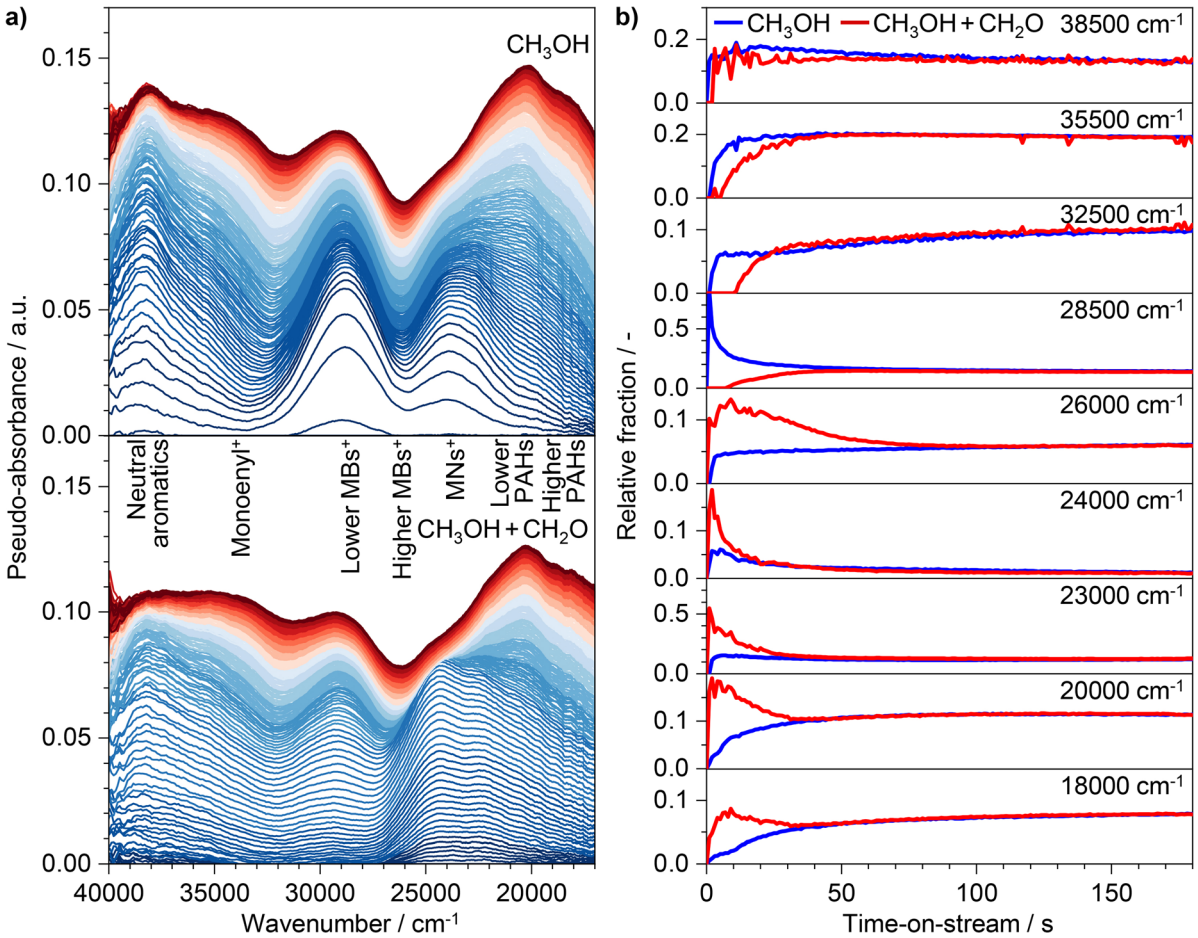

Fig. 7 (a) DR-UV/vis spectra of Z_{40} during the MTH reaction in the absence (top) and in the presence (bottom) of formaldehyde in the feed. (b) Temporal evolution of the relative fractions of specific spectral components obtained by deconvolution into the Gaussian peaks as indicated in Fig. S10.† Reaction conditions: $CH_3OH : CH_2O : Ar$ = 10.6 : 0(0.2) : 89.4(89.2) mol%, WHSV = 41 g_{CH_3OH} g_{cat}^{-1} h^{-1}, T = 673 K, and P = 1.2 bar.

onset of arene formation are consistent with the proposed reaction sequential reaction scheme (Fig. 4b, top scheme).

To complement the above findings, DR-UV/vis spectroscopy was applied to monitor the evolution of the reaction intermediates in the zeolite pores induced by the addition of formaldehyde to the MTH reaction over the Z_{40} catalyst (Fig. 7 and S10†). In agreement with previous reports,[45–47] the bands centered at *ca.* 35 500 and 32 500 cm^{-1}, attributed to monoenyl carbenium ions (cyclic and acyclic), the band centered at *ca.* 28 500 cm^{-1} associated with lower MB and/or dienyl (cyclic and acyclic) carbenium ions, and the band centered at *ca.* 26 000 cm^{-1}, associated with higher MB carbenium ions, represent the prevailing spectral features in the early stage of the MTH reaction (Fig. 7a, top). Higher-wavelength spectral components associated with MNs (*ca.* 23 000 cm^{-1}), and lower (*ca.* 20 000 cm^{-1}) and higher (*ca.* 18 000 cm^{-1}) polycyclic aromatic hydrocarbons (PAHs), *i.e.*, coke precursors and species, increase as the reaction progresses (Fig. 7b).[45–47] A significantly different behavior is obtained if only a small amount of formaldehyde is co-fed with methanol ($CH_3OH : CH_2O$ = 10.6 : 0.2 mol%, Fig. 7a, bottom). The relative fraction of the bands associated with the monoenyl carbenium ion components was very low at the start of the reaction, whereas the signals associated with MBs, and especially with MNs and PAHs, intensified immediately after the reaction started. These spectral profiles indicate that formaldehyde greatly enhances the conversion of monoenyl and dienyl species into MBs and further into MNs and coke species, which is consistent with the product evolution profiles observed in the PEPICO experiments.

Formaldehyde-mediated reactions

PEPICO analysis of formaldehyde formation in the early stage of MTH conversion revealed that the formation of this primary reaction product proceeds with an apparent activation barrier of 70 kJ mol^{-1}. This value is comparable to the apparent activation barriers of the methylation and cracking steps of the DCHP mechanism (40–80 kJ mol^{-1}),[36–39] indicating that the formaldehyde formation is competitive with the formation of the hydrocarbon products during the MTH reaction.

The formaldehyde concentration profiles recorded over Z_{15} and Z_{40} and their steamed sZ_{15} and sZ_{40} counterparts

demonstrate the higher reactivity of formaldehyde over catalysts with higher propensity to coking. Therefore, a faster decrease in the formaldehyde yield over Z_{15} with respect to Z_{40} at constant τ_{BAS}, as well as over sZ_{15} with respect to the Z_{40} material, despite the lower BAS concentration in the former (Fig. 3b), indicates that the nature of BAS and, potentially, of the LAS and framework defects such as silanols also affects the reactivity of formaldehyde in addition to the concentration. Moreover, the correlations between a decrease in formaldehyde and alkene yield and an increase in dienes corroborate the proposal that FMRs are initiated by the formation of the latter products from alkenes *via* Prins condensation. In this respect, higher yields of dienes over more stable catalysts that are also less reactive towards formaldehyde (*e.g.*, Z_{40} *vs.* Z_{15}, sZ_{15} and sZ_{40} *vs.* Z_{15} and sZ_{40}) suggest the importance of the diene–formaldehyde reactions in the formation of aromatics and coke (Fig. 4b, top scheme). Both PEPICO and DRUV-vis analyses indicate high dienyl and, especially, cyclopentadienyl intermediate reactivity with formaldehyde, which correlates with the enhancement in the production rates of higher MNs and PAHs. The critical role of more conjugated triene products and their cyclic derivatives, cyclopentadienyl species, in promoting catalyst deactivation is also supported by the much higher deactivation potential of hexatriene and cyclopentadiene co-feeds with respect to analogues hexadiene and methylcyclohexene feeds at similar concentration levels (Fig. 8 and S11†). Notably, the PEPICO spectra indicate the formation of fulvene derivatives, which can be obtained *via* Prins condensation from cyclopentadiene and can readily isomerize into benzene rings (Fig. 4b, top scheme). This enables the prompt buildup of arene chain carriers. These observations indicate that the critical role of formaldehyde in the MTH mechanism originates primarily from its ability to enhance the formation of longer conjugated hydrocarbons and arene rings *via* condensation reactions that bypass the HT steps.

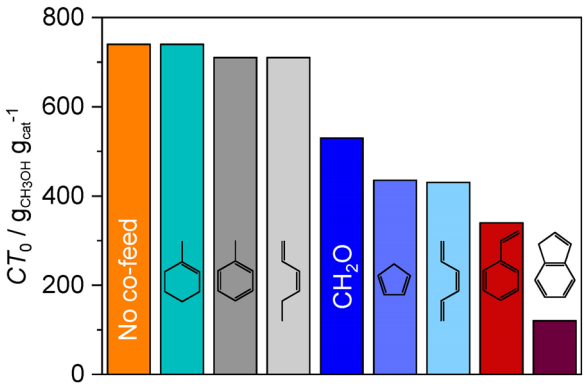

Fig. 8 Cumulative turnover capacities of the Z_{40} catalyst in the MTH reaction in the presence of different co-feeds. All reactants and products were detected and quantified by the GC-FID method. Reaction conditions: CH_3OH : co-feed : Ar = 21 : 0.4(0) : 88.6(89) mol%, WHSV = 76 g_{CH_3OH} g_{cat}^{-1} h^{-1}, T = 673 K, and P = 1.6 bar.

In addition to the enhancement of the alkene–polyene–MBs reaction cascade, PEPICO experiments indicate that other higher molecular weight species are formed in FMRs. In particular, the observation of signals attributed to indene and styrene derivatives indicates that formaldehyde enhances the stepwise growth of polycyclic aromatics, potentially *via* side-chain condensation reactions that generate the unsaturated alkenyl substituents that can undergo cyclization reactions (Fig. 4b, top scheme). Styrene and especially indene species exhibit strong catalyst deactivation potential, as demonstrated by co-feeding of small amounts of these hydrocarbons over the Z_{40} catalyst (Fig. 8 and S10†). Finally, the formation of MNs may proceed *via* cyclization of the vinyl substituents of divinylbenzene species (Fig. 4b, top scheme).

Conclusions

This study provides an in-depth assessment of formaldehyde formation and transformation in the MTH reaction over practically relevant ZSM-5 catalysts and their contributions to catalyst deactivation. In the early stage of the MTH reaction, formaldehyde formation mainly proceeds *via* methanol disproportionation, with an apparent activation energy of *ca.* 70 kJ mol^{-1}. This value is comparable to the activation barriers of the methylation steps in the DCHP reaction sequences, indicating that formaldehyde formation is competitive with the evolution of hydrocarbon products. The formaldehyde yield profiles indicate that it primarily reacts with alkenes, transforming them into (cyclo)dienes with increasing reactivity as a function of alkene size. This is followed by the prompt conversion of dienes into aromatics, wherein cyclopentadienes are particularly reactive towards formaldehyde. The detection of fulvenes, which can be produced *via* Prins condensation of cyclopentadienes with formaldehyde and may isomerize into MBs, suggests that they can be the intermediates between dienes and arenes. The prominent build-up of styrene, indene, and naphthalene derivatives in the presence of formaldehyde co-feeds implies that condensation of the side chain-substitutes with formaldehyde, coupled with ring closure reactions of the obtained alkenyl, constitutes a possible reaction pathway leading to the formation of PAHs, *i.e.*, coke. The measured product distribution profiles over the ZSM-5 catalysts demonstrate a positive correlation between formaldehyde reactivity and catalyst propensity to coking. Herein, the formaldehyde-mediated reactions are not only dependent on the concentration of the BAS but also on their speciation and are likely affected by the LAS and framework-associated defects such as silanols. The results evidence an important role of formaldehyde in the reaction sequences causing deactivation of the MTH catalysts.

Experimental

Catalysts and characterization

ZSM-5 catalysts with nominal Si/Al ratios of 15 (Zeolyst, CBV 3024E) and 40 (Zeolyst, CBV 8014), labeled Z_{15} and Z_{40},

respectively, were received in the ammonium form and transformed into their protonic form by calcination. Calcium-modified ZSM-5 with a nominal loading of 1 wt%, denoted as CaZ_{40}, was prepared by dry impregnation of the ammonium form of Z_{40} using an aqueous solution of $Ca(NO_3)_2{\cdot}4H_2O$ (Sigma-Aldrich, >99%), followed by drying in a vacuum (30 mbar) at 353 K for 12 h. Severely steamed ZSM-5 catalysts, labeled sZ_{15} and sZ_{40}, were prepared by steaming the Z_{15} and Z_{40} parent materials, respectively, in a quartz fixed-bed reactor at 773 K for 5 h using a feed of H_2O : Ar = 18 : 72 mol% and a weight-hourly space velocity (WHSV) of 10.2 g_{H_2O} g_{cat}^{-1} h^{-1}. All catalysts were calcined under an oxygen flow (PanGas 5.0, F_{O_2} = 100 cm^3_{STP} min^{-1}) at 823 K for 5 h at a heating rate of 2 K min^{-1}. The materials were characterized by powder X-ray diffraction (PXRD), scanning electron microscopy with energy dispersive X-ray analysis (SEM–EDX), ^{27}Al magic angle spinning nuclear magnetic resonance (^{27}Al MAS NMR), and Fourier transform infrared spectroscopy (FTIR), as detailed in the ESI.†

Catalyst testing in the MTH conversion

MTH catalytic tests were performed in a continuous-flow fixed-bed reactor setup using a methanol (CH_3OH, Sigma-Aldrich, ≥99.9%) in argon (PanGas, 5.0) feed at a molar ratio of CH_3OH : Ar = 19 : 81 mol%, WHSV = 25, 76, or 253 g_{CH_3OH} g_{cat}^{-1} h^{-1} at T = 673 or 773 K, and P = 1.6 bar. Details of the reactor setup, catalytic tests, and analysis protocols are provided in the ESI.†

PEPICO spectroscopy experiments

Species exiting the MTH reactor were analyzed using PEPICO spectroscopy at the vacuum ultraviolet (VUV) beamline of the Swiss Light Source (Fig. S1†).[31,48–50] Argon (used as a diluent) and xenon (Xe, 2% in Ar, Messer, 5.0, used as an internal calibrant) were fed using digital mass flow controllers (MKS). Diluted methanol vapor and ^{13}C-labeled methanol ($^{13}CH_3OH$, Sigma-Aldrich, 99 atom% ^{13}C) were introduced by passing the argon flow through a methanol bubbler, placed in a water thermostat maintained at a constant temperature of 278 K. The diluted formaldehyde feed was prepared by passing the argon flow through a small vessel loaded with 1,3,5-trioxane flakes (Sigma-Aldrich, ≥99%), which acted as an anhydrous source of this aldehyde. Four-way valves were used to direct the reactive feed to an exhaust vacuum line for stabilization or to the MTH reactor, as well as to introduce formaldehyde into the methanol feed. All catalytic tests were performed in a quartz reactor (d_i = 4 mm) with an outlet pinhole. The zeolite catalysts (W_{cat} = 6–24 mg, d_p = 0.18–0.25 mm) were well mixed with quartz particles (Thommen-Furler, washed in HNO_3 and calcined, d_p = 0.355–0.420 mm) and loaded in the form of a fixed bed between two thin layers of quartz wool. The tip of a type K thermocouple was placed in the center of the catalyst bed and used to monitor the reaction temperature. The reactor temperature was controlled using a home-made, resistively heated electric oven, which was connected to two type K thermocouples and a PID controller. The reaction pressure was monitored using a pressure transducer above the reaction zone. Prior to the experiment, the reactors were thermally treated under an argon flow at 773 K for 0.5 h to remove any potential organic impurities. Unless otherwise stated, the MTH reaction was conducted using a reaction mixture of the composition CH_3OH : CH_2O : Xe : Ar = 1.95 : 0(1.1) : 0.15 : 97.9(96.8) mol%, WHSV of 1.4, 3.4, or 5.4 g_{CH_3OH} g_{cat}^{-1} h^{-1}, T = 537–727 K, and P = 0.4 bar.

The molecular beam leaving the reactor was skimmed as it entered the ionization chamber, operating at 2×10^{-9} bar. There, it was ionized by VUV synchrotron radiation. The radiation was dispersed by a 150 mm^{-1} grating working in grazing incidence and focused at the 200 μm exit slit in a rare gas filter to monochromatize it. Higher order radiation of the grating was suppressed in the 9–14 eV photon energy range by using a Ne : Ar : Kr mixture in the gas filter (Messer, Ne : Ar : Kr = 60 : 30 : 10 mol%), operating at 8×10^{-3} bar over an optical length of 10 cm. The photoions and photoelectrons generated by photoionization were accelerated vertically in opposite directions by a constant electric field (213 V cm^{-1}) towards two delay-line anode detectors (Roentdek, DLD40), where they were velocity map imaged and detected in delayed coincidence. Further details of the methanol and product analyses are provided in the ESI.†

DRUV-vis spectroscopy experiments

Surface-confined MTH reaction intermediates were studied by *operando* diffuse reflectance UV-visible (DRUV-vis) spectroscopy using a home-built plug-flow reactor cell closed with a calcium fluoride window and connected to a GC-FID analyzer (Fig. S1†).[51] Spectra were recorded with a fiber optic spectrometer (AvaSpec ULS2048CL, Avantes) combined with a deuterium halogen light source (Avalight-DHS, Avantes) and a reaction probe (FCR-7UVIR600, Avantes) placed in front of the calcium fluoride window perpendicular to the reactor. Formaldehyde (CH_2O, 23.5% in water, methanol-free, Roth) was dissolved in methanol. MTH catalytic tests were performed using a feed of CH_3OH : CH_2O : Ar = 10.6 : 0(0.2) : 89.4(89.2) mol%, WHSV = 41 g_{CH_3OH} g_{cat}^{-1} h^{-1} at T = 673 K, and P = 1.2 bar. Further details of the DRUV-vis setup and data analysis are provided in the ESI.†

Author contributions

V. P. conceived the idea, performed the i^2PEPICO and UV-vis experiments and MTH catalytic tests, analyzed the data, and coordinated this project. X. W., P. H. and A. B. supported the planning and execution of the i^2PEPICO experiments and the analysis of the obtained spectra, and discussed the i^2PEPICO data. L. M. and D. F. supported the execution of the UV-vis experiments and the spectra analysis. J. A. v. B. acquired funding and discussed the data. V. P. wrote the manuscript with comments and corrections from all the authors.

Conflicts of interest

There are no conflicts to declare.

Acknowledgements

We acknowledge the VUV beamline of the Swiss Light Source at the Paul Scherrer Institute (PSI), Villigen, Switzerland for granting a beamtime, Dr. Zeyou Pan and Mr. Patrick Ascher from the PSI for technical assistance during the i^2PEPICO measurements, Dr. Przemyslaw Rzepka from ETH Zurich and the Paul Scherrer Institute for help with SEM–EDX analysis, ScopeM at ETH Zurich for the access to the SEM facility, and the Energy System Integration platform of the PSI for financial support. L. M. and D. F. would like to thank the ETH Board (Switzerland) for financial support through the program 'SynFuels – Synthetic Fuels from Renewable Resources'.

References

1 U. Olsbye, S. Svelle, M. Bjrgen, P. Beato, T. V. W. Janssens, F. Joensen, S. Bordiga and K. P. Lillerud, *Angew. Chem., Int. Ed.*, 2012, **51**, 5810–5831.
2 P. Tian, Y. Wei, M. Ye and Z. Liu, *ACS Catal.*, 2015, **5**, 1922–1938.
3 I. Yarulina, A. D. Chowdhury, F. Meirer, B. M. Weckhuysen and J. Gascon, *Nat. Catal.*, 2018, **1**, 398–411.
4 S. Ilias and A. Bhan, *ACS Catal.*, 2013, **3**, 18–31.
5 V. Van Speybroeck, K. De Wispelaere, J. Van Der Mynsbrugge, M. Vandichel, K. Hemelsoet and M. Waroquier, *Chem. Soc. Rev.*, 2014, **43**, 7326–7357.
6 V. Paunović, V. Sushkevich, P. Rzepka, L. Artiglia, R. Hauert, S. Sik Lee and J. A. van Bokhoven, *J. Catal.*, 2022, **407**, 54–64.
7 J. Valecillos, H. Vicente, A. G. Gayubo, A. T. Aguayo and P. Castaño, *J. Catal.*, 2022, **408**, 115–127.
8 K. Barbera, S. Sørensen, S. Bordiga, J. Skibsted, H. Fordsmand, P. Beato and T. V. W. Janssens, *Catal. Sci. Technol.*, 2012, **2**, 1196.
9 Y. Wei, C. Yuan, J. Li, S. Xu, Y. Zhou, J. Chen, Q. Wang, L. Xu, Y. Qi, Q. Zhang and Z. Liu, *ChemSusChem*, 2012, **5**, 906–912.
10 J. S. Martinez-Espin, M. Mortén, T. V. W. Janssens, S. Svelle, P. Beato and U. Olsbye, *Catal. Sci. Technol.*, 2017, **7**, 2700–2716.
11 S. Lee and M. Choi, *J. Catal.*, 2019, **375**, 183–192.
12 S. Müller, Y. Liu, M. Vishnuvarthan, X. Sun, A. C. van Veen, G. L. Haller, M. Sanchez-Sanchez and J. A. Lercher, *J. Catal.*, 2015, **325**, 48–59.
13 B. L. Foley, B. A. Johnson and A. Bhan, *ACS Catal.*, 2021, **11**, 3628–3637.
14 Y. Liu, S. Müller, D. Berger, J. Jelic, K. Reuter, M. Tonigold, M. Sanchez-Sanchez and J. A. Lercher, *Angew. Chem., Int. Ed.*, 2016, **55**, 5723–5726.
15 S. Müller, Y. Liu, F. M. Kirchberger, M. Tonigold, M. Sanchez-Sanchez and J. A. Lercher, *J. Am. Chem. Soc.*, 2016, **138**, 15994–16003.
16 J. S. Martínez-Espín, K. De Wispelaere, T. V. W. Janssens, S. Svelle, K. P. Lillerud, P. Beato, V. Van Speybroeck and U. Olsbye, *ACS Catal.*, 2017, **7**, 5773–5780.
17 Y. Liu, F. M. Kirchberger, S. Müller, M. Eder, M. Tonigold, M. Sanchez-Sanchez and J. A. Lercher, *Nat. Commun.*, 2019, **10**, 1462.
18 L. Kilburn, M. DeLuca, A. J. Hoffman, S. Patel and D. Hibbitts, *J. Catal.*, 2021, **400**, 124–139.
19 F. M. Kirchberger, Y. Liu, P. N. Plessow, M. Tonigold, F. Studt, M. Sanchez-Sanchez and J. A. Lercher, *Proc. Natl. Acad. Sci. U. S. A.*, 2022, **119**, 1–10.
20 V. Paunović, P. Hemberger, A. Bodi, R. Hauert and J. A. van Bokhoven, *ACS Catal.*, 2022, **12**, 13426–13434.
21 Y. Ni, W. Zhu and Z. Liu, *ACS Catal.*, 2019, **9**, 11398–11403.
22 A. Hwang and A. Bhan, *ACS Catal.*, 2017, **7**, 4417–4422.
23 S. S. Arora, D. L. S. Nieskens, A. Malek and A. Bhan, *Nat. Catal.*, 2018, **1**, 666–672.
24 S. S. Arora, Z. Shi and A. Bhan, *ACS Catal.*, 2019, **9**, 6407–6414.
25 J. S. Martinez-Espin, K. De Wispelaere, M. Westgård Erichsen, S. Svelle, T. V. W. Janssens, V. Van Speybroeck, P. Beato and U. Olsbye, *J. Catal.*, 2017, **349**, 136–148.
26 S. M. T. Almutairi, B. Mezari, E. A. Pidko, P. C. M. M. Magusin and E. J. M. Hensen, *J. Catal.*, 2013, **307**, 194–203.
27 T. Liang, J. Chen, Z. Qin, J. Li, P. Wang, S. Wang, G. Wang, M. Dong, W. Fan and J. Wang, *ACS Catal.*, 2016, **6**, 7311–7325.
28 I. Yarulina, K. De Wispelaere, S. Bailleul, J. Goetze, M. Radersma, E. Abou-Hamad, I. Vollmer, M. Goesten, B. Mezari, E. J. M. Hensen, J. S. Martínez-Espín, M. Morten, S. Mitchell, J. Perez-Ramirez, U. Olsbye, B. M. Weckhuysen, V. Van Speybroeck, F. Kapteijn and J. Gascon, *Nat. Chem.*, 2018, **10**, 804–812.
29 J. Krüger, G. A. Garcia, D. Felsmann, K. Moshammer, A. Lackner, A. Brockhinke, L. Nahon and K. Kohse-Höinghaus, *Phys. Chem. Chem. Phys.*, 2014, **16**, 22791–22804.
30 P. Hemberger, V. B. F. Custodis, A. Bodi, T. Gerber and J. A. van Bokhoven, *Nat. Commun.*, 2017, **8**, 15946–15955.
31 B. Sztáray, K. Voronova, K. G. Torma, K. J. Covert, A. Bodi, P. Hemberger, T. Gerber and D. L. Osborn, *J. Chem. Phys.*, 2017, **147**, 13944–13954.
32 P. Hemberger, J. A. Van Bokhoven, J. Pérez-Ramírez and A. Bodi, *Catal. Sci. Technol.*, 2020, **10**, 1975–1990.
33 A. Cesarini, S. Mitchell, G. Zichittella, M. Agrachev, S. P. Schmid, G. Jeschke, Z. Pan, A. Bodi, P. Hemberger and J. Pérez-Ramírez, *Nat. Catal.*, 2022, **5**, 605–614.
34 A. Liutkova, H. Zhang, J. F. M. Simons, B. Mezari, M. Mirolo, G. A. Garcia, E. J. M. Hensen and N. Kosinov, *ACS Catal.*, 2023, **13**, 3471–3484.
35 S. G. Lias, J. E. Bartmess, J. F. Liebman, J. L. Holmes, R. Levin and W. G. Mallard, in *NIST Chemistry WebBook, NIST Standard Reference Database Number 69*, ed. P. J. Linstrom and W. G. Mallard, National Institute of Standards and Technology, 2023.

36 I. M. Hill, Y. S. Ng and A. Bhan, *ACS Catal.*, 2012, **2**, 1742–1748.
37 I. Hill, A. Malek and A. Bhan, *ACS Catal.*, 2013, **3**, 1992–2001.
38 V. Van Speybroeck, J. Van Der Mynsbrugge, M. Vandichel, K. Hemelsoet, D. Lesthaeghe, A. Ghysels, G. B. Marin and M. Waroquier, *J. Am. Chem. Soc.*, 2011, **133**, 888–899.
39 L. Qi, Y. Wei, L. Xu and Z. Liu, *ACS Catal.*, 2015, **5**, 3973–3982.
40 S. Ilias, R. Khare, A. Malek and A. Bhan, *J. Catal.*, 2013, **303**, 135–140.
41 M. Bjørgen, F. Joensen, M. Spangsberg Holm, U. Olsbye, K. P. Lillerud and S. Svelle, *Appl. Catal., A*, 2008, **345**, 43–50.
42 S. M. Campbell, D. M. Bibby, J. M. Coddington and R. F. Howe, *J. Catal.*, 1996, **161**, 350–358.
43 K. Barbera, F. Bonino, S. Bordiga, T. V. W. Janssens and P. Beato, *J. Catal.*, 2011, **280**, 196–205.
44 R. I. Kaiser, L. Zhao, W. Lu, M. Ahmed, M. V Zagidullin, V. N. Azyazov and A. M. Mebel, *J. Phys. Chem. Lett.*, 2022, **13**, 208–213.
45 D. Mores, E. Stavitski, M. H. F. Kox, J. Kornatowski, U. Olsbye and B. M. Weckhuysen, *Chem. – Eur. J.*, 2008, **14**, 11320–11327.
46 J. Goetze, F. Meirer, I. Yarulina, J. Gascon, F. Kapteijn, J. Ruiz-Martínez and B. M. Weckhuysen, *ACS Catal.*, 2017, **7**, 4033–4046.
47 D. Fu, O. Heijden, K. Stanciakova, J. E. Schmidt and B. M. Weckhuysen, *Angew. Chem., Int. Ed.*, 2020, **59**, 15502–15506.
48 A. Bodi, B. Sztáray, T. Baer, M. Johnson and T. Gerber, *Rev. Sci. Instrum.*, 2007, **78**, 084102.
49 D. L. Osborn, C. C. Hayden, P. Hemberger, A. Bodi, K. Voronova and B. Sztáray, *J. Chem. Phys.*, 2016, **145**, 164202.
50 A. Bodi, M. Johnson, T. Gerber, Z. Gengeliczki, B. Sztáray and T. Baer, *Rev. Sci. Instrum.*, 2009, **80**, 034101.
51 G. L. Chiarello, M. Nachtegaal, V. Marchionni, L. Quaroni and D. Ferri, *Rev. Sci. Instrum.*, 2014, **85**, 074102.